Letters

Vulnerability of a VOC-Based Inverter Due to Noise Injection and Its Mitigation

Sourojit K. Mazumder, Mateo D. Roig Greidanus, *Graduate Student Member, IEEE*, Ji Liu, *Member, IEEE*, and H. Alan Mantooth, *Fellow, IEEE*

***Abstract*—Even though virtual oscillator control (VOC)-based inverters do not communicate with each other, they need to make local measurements for control. The impact of tampering with these measured or sensed signals on the performance of a VOC-based inverter and synchronization of multiple such inverters is an important but open-ended issue. As such, this letter explores the impact of intentional side-channel noise intrusion (SNI) on the synchronization of VOC-based communication-free self-synchronizing inverters (CFSIs). Two different scenarios are investigated via experimental and analytical studies using a half-bridge neutral point clamped (NPC) single-phase CFSI. They address the impact of SNI on the ability of a CFSI to ensure a stable 60-Hz limit cycle and on the parallel operation of two such CFSIs to ensure synchronism to a common 60-Hz load frequency.**

***Index Terms*—Inverter, noise, oscillator, synchronization, virtual oscillator control (VOC).**

I. Introduction

RECENTLY, the authors in [1] explored the impact of side-channel noise intrusion (SNI) on the performance of a communication-based inverter (CBI) and how such noise injection can lead to subsynchronous inverter output. While CBI has been the workhorse of the power-electronics industry, recently self-synchronizing communication-free self-synchronizing inverter (CFSIs), based on virtual oscillator control (VOC) [2], have gained traction. This is mainly because they operate in a decentralized fashion without information exchange and can scale in network size without their performances affected by communication latency.

Manuscript received 5 August 2022; revised 14 September 2022; accepted 6 October 2022. Date of publication 19 October 2022; date of current version 18 November 2022. This material is based in part upon work supported by the U.S. Department of Energy's Office of Energy Efficiency and Renewable Energy (EERE) under the Solar Energy Technology Office (SETO) Award Number DE-EE0009026. *(Corresponding author: Sourojit K. Mazumder.)*

Sourojit K. Mazumder is with the William Fremd, Hoffman Estates, IL 60067 USA (e-mail: sourojitmazumder@gmail.com).

Mateo D. Roig Greidanus is with the Electrical and Computer Engineering Department, University of Illinois at Chicago, Chicago, IL 60607 USA (e-mail: mgreid2@uic.edu).

Ji Liu is with the Electrical and Computer Engineering, Stony Brook University College of Engineering and Applied Sciences, Stony Brook, NY 11794 USA (e-mail: ji.liu@stonybrook.edu).

H. Alan Mantooth is with the Electrical Engineering, University of Arkansas Fayetteville, Fayetteville, AR 72701 USA (e-mail: mantooth@uark.edu).

Color versions of one or more figures in this article are available at https://doi.org/10.1109/TPEL.2022.3214835.

Digital Object Identifier 10.1109/TPEL.2022.3214835

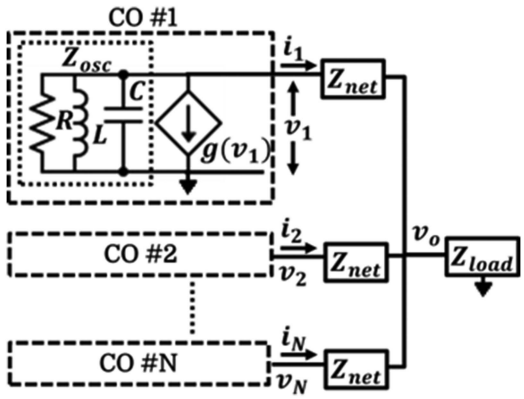

Fig. 1. Illustration of N COs feeding a load (Z_{load}) via network impedances (Z_{net}). Further, for all COs $g(v) = f(v) - \sigma v$ and $f(v) = 2\sigma(v \mp \varphi)$ if $\pm v > \varphi$ or $f(v) = 0$ [2].

While such VOC-based CFSIs do not use a data network for communication, they do use local measurements for implementing control. So, an open-ended issue, in this regard, is to assess the efficacy of VOC-based CFSI if such measurements are tampered with using SNI as motivated by [1], [3], and references therein. Specifically, and unlike [1], we investigate the effect of SNI on the ability of an inverter to ensure a stable 60-Hz limit cycle and the impact of SNI on the parallel operation of such CFSIS to ensure synchronism to a common 60-Hz load frequency. Section II captures the background regarding the condition for synchronization of coupled oscillators (COs). Section III outlines how VOC-based CFSIs can be synchronized as COs and the incorporation of SNI in the feedback current. Section IV investigates experimentally the impact of SNI on the performance of a single-phase half-bridge NPC-based CFSI and, subsequently, on two such CFSIs connected in a parallel configuration. Finally, in Section V, the relevant conclusions are provided.

II. Condition for Synchronization of Nonlinear COs

Reference [2] outlines that a network of N identical nonlinear COs, as illustrated in Fig. 1, synchronizes in the sense of (1) if the condition (A3) is satisfied

$$\lim_{v \to \infty} v_j(t) - v_k(t) = 0 \;\; \forall j,\; k = 1, \cdots N \tag{1}$$

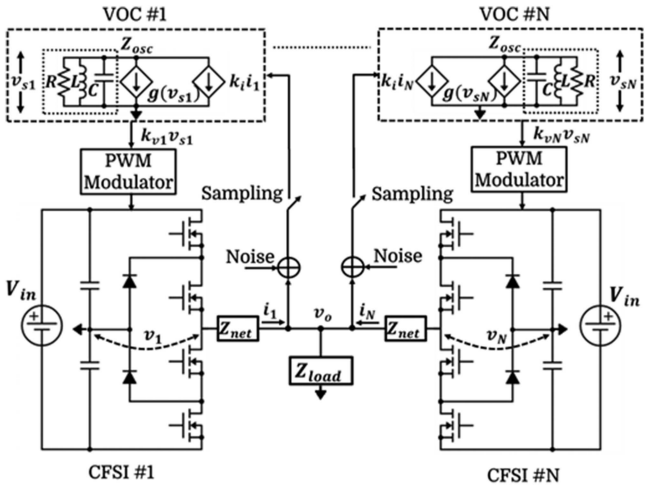

Fig. 2. VOC-based (half-bridge-NPC) CFSIs operating as COs emulating the network structure shown in Fig. 1, where $k_{vx} v_{sx}$ ($\forall x = 1, \cdots, N$) represents the xth modulating signal.

where $v_j(t)$ represents the output voltage of the jth CO. Further, it follows from Lienard's theorem [4] that an oscillator system described by the following:

$$\ddot{v} + r(v)\,\dot{v} + m(v) = 0. \tag{2}$$

with symbols defined in Appendix B, has a unique and stable limit cycle if conditions (B2)–(B5) are satisfied. An electrical realization of (2) [2] is shown in Fig. 1 for an oscillator which needs to satisfy $\omega_o = (LC)^{-1/2}$ (synchronizing angular frequency), $\epsilon = \sqrt{LC^{-1}}(\sigma - R^{-1})$ is minimized (to realize a circular phase plane), and $\sigma > R^{-1}$ (for stable limit cycle).

III. VOC-Based CFSI for Synchronized CO and SNI

To operate a network of (half-bridge NPC [5]) CFSIs like a network of COs at 60 Hz, as illustrated in Fig. 1, each such CFSI is controlled using a VOC, which is implemented in a digital–signal–processor-based platform. However, unlike the CO in Fig. 1 that powers the load directly, in Fig. 2, it is the CFSI that powers the load. Hence, a scaled value of the output current (e.g., $k_i i_1$ and $k_i i_N$ for the first and the Nth CFSI) provided by a CFSI to the load is fed to the corresponding VOC to close the control loop.

Injection of SNI in the CFSI current feedback, as illustrated in Fig. 2, may negatively affect the performance of the inverter and the inverter network. The mechanism to inject such noise has been indicated in [1], [3] for non-VOC-based inverters and references therein. However, unlike [1], the VOC [2], which behaves like a bandpass filter (centered around the 60-Hz load frequency), is less sensitive to the frequency of SNI outside the bandwidth of the filter. Based on Section II, it is obvious that a larger value of R, for a given σ, yields a larger ϵ. This yields higher distortion in the limit cycle waveform (or CFSI output) [2] even though the bandwidth of the VOC bandpass filter is narrower. In contrast, a smaller value of R, per Section II, makes the limit cycle (or the CFSI output) more vulnerable to instability [2] even though it yields lower ϵ that yields lower distortion in CFSI output. In addition, it yields a higher bandwidth of the VOC bandpass filter.

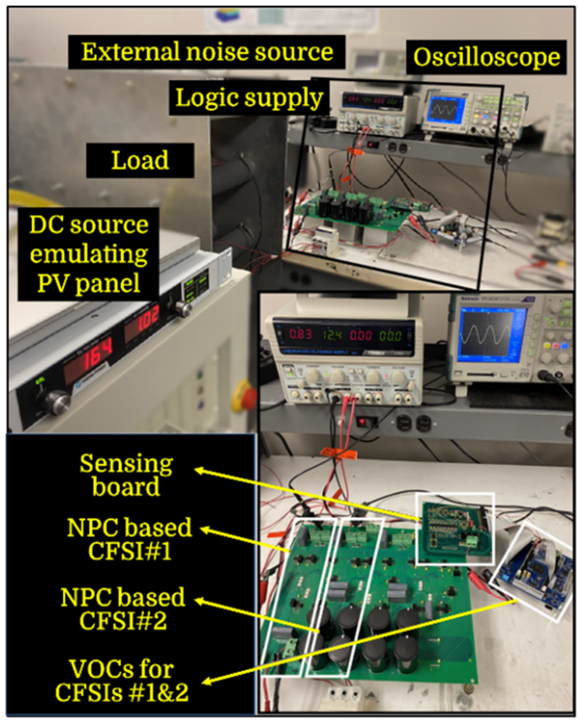

Fig. 3. Experimental setup of the single-phase half-bridge NPC-based CFSI.

IV. Impact of SNI on a VOC-Based CFSI Limit Cycle

To begin with, we explore the impact of injecting noise on the stability of the 60-Hz limit cycle associated with a CFSI output. The experimental setup for the single-phase half-bridge NPC-based CFSI is shown in Fig. 3. The relevant nominal parameters for the half-bridge CFSI are as follows that also ensure the synchronization condition (without SNI), as outlined in [2] (and briefly captured in Section II) is satisfied as well:

- output frequency: 60 Hz (yields $T_{60} = 1/60$ s);
- output voltage: 75 V;
- input dc voltage (V_{in}): 170 V;
- switching frequency: 20 kHz;
- sampling frequency: 20 kHz;
- Z_{net} (R_{net}, L_{net}, C_{net}): 67 mΩ, 500 μH, 3.9 μF;
- Z_{load}: 20 Ω;
- Z_{osc} (R, L, C): 10 Ω, 500 μH, 14.07 mF;
- $\sigma = 1$, $\varphi = 0.4695$, $k_i = 0.04$, $k_v = 72.25$.

Fig. 4 experimentally investigates the impact of SNI in i_1 (as illustrated in Fig. 2) on the performance of a CFSI. Based on the Z_{osc} parameters based on its circuit configuration shown in Fig. 2, the nominal bandwidth of the bandpass filter (centered at 60 Hz) is determined to be 7.1 Hz. As such, an SNI frequency of 57 Hz, which is close to the bandwidth of the filter is selected, and the amplitude of the noise is set at 100% of the nominal i_1.

To differentiate the impact of the SNI from the nominal performance of the CFSI, Fig. 4(a) shows a baseline open-loop (OL) and VOC-based performances of the inverter without

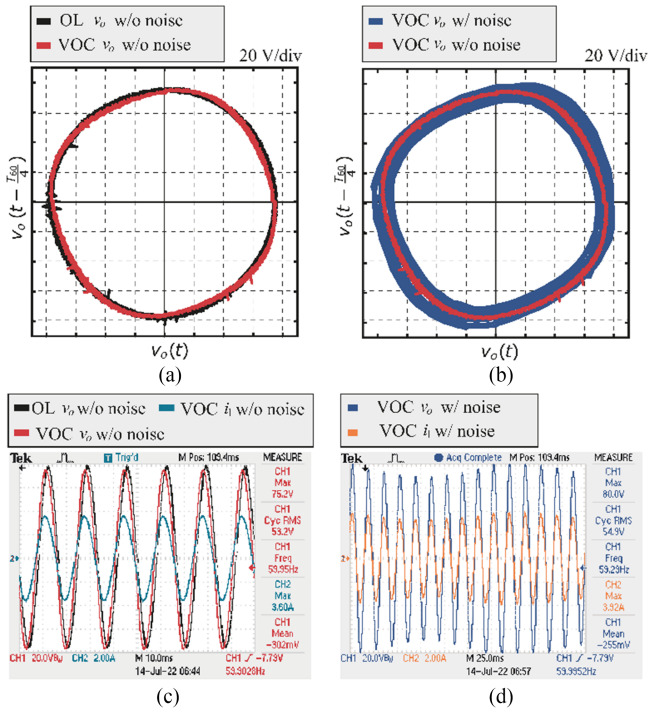

Fig. 4. Performance of a single CFSI without and with SNI. (a), (b) Using phase-plane plots of v_o. (c), (d) Using time-domain plots of v_o and i_1. Further, (a), (c) Capture dynamics without SNI. (b), (d) Capture dynamics with SNI.

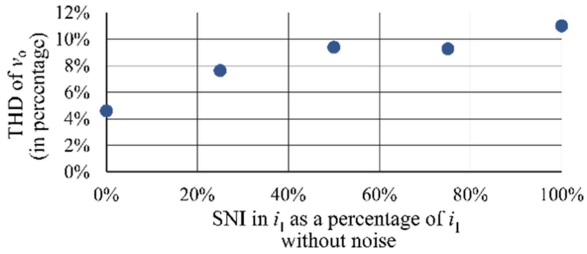

Fig. 5. Increasing THD of v_o with increasing SNI (at 57 Hz) in i_1.

noise. Since the CFSI is a single-phase inverter, a phase-plane plot (that captures the limit cycle) is captured by plotting $v_o(t)$ against $v_o(t - T_{60}/4)$. The slight variation in the VOC-based performance (compared to the OL performance) is attributed to the choice of ϵ [2], which controls the limit cycle's deviation from an ideal circular profile.

Fig. 4(b) shows the impact of SNI on v_o of the CFSI. It is evident that the noise injection disturbs the periodic dynamics of the inverter (obtained without noise), and the CFSI is no more able to synchronize to the fundamental 60-Hz output frequency for which the VOC was tuned. This is evident in the loss of the 60-Hz limit cycle. This deviation is also evident if one compares the time-domain (v_o and i_1) plots shown in Fig. 4(c) and 4(d) corresponding to the cases with and without SNI. The loss of the 60-Hz operation is also evident in Fig. 4(d).

Fig. 5 shows an experimental parametric plot that captures the impact of the SNI in i_1 on v_o. Fig. 5 shows that with the SNI, the total harmonic distortion (THD) of v_o is higher than that obtained without SNI. The minor deviation in THD with increasing noise is attributed to the fact that, with SNI, since the periodicity of the 60-Hz cycle is lost; the calculation of the THD can be obtained only in an approximate sense [6].

Having demonstrated the impact of SNI at a noise frequency close to the resonant frequency of the VOC impedance experimentally, we now explore the impact of variation analytically in SNI noise frequency with varying VOC bandwidth and noise amplitude. The averaged model of the VOC-based half-bridge ANPC inverter (ignoring parasitics and noting that Z_{net} is an LC filter) is captured by (3) where i_N is the noise

$$L_{\text{net}}\dot{i}_{L\text{net}}/dt = dV_{\text{in}} - v_{C\text{net}};(d = k_v v_{s1},\ v_o = v_{C\text{net}}) \quad (3a)$$

$$C_{\text{net}}dv_{C\text{net}}/dt = i_{L\text{net}} - v_{C\text{net}}/Z_{\text{load}} \quad (3b)$$

$$L\dot{i}_L/dt = v_C = v_{s1} \quad (3c)$$

$$Cdv_C/dt = -g\left(v_C\right) - k_i\left(v_{C\text{net}}/Z_{\text{load}} + i_N\right) - i_L - v_C/R \quad (3d)$$

where $g(.)$ is outlined in [2] and illustrated in Fig. 1. Equations 3(a)–3(d) shows that without noise (i.e., $i_N = 0$), one of the equilibrium solutions is the origin. However, this is not the equilibrium one desires in a VOC-based inverter model and instead one seeks a period-one orbit (limit cycle) [2]. Using the Lyapunov function 4(a) and its derivative 4(b) obtained using 3(a)–3(d)

$$V = \frac{1}{2}L_{\text{net}}i_{L\text{net}}^2 + \frac{1}{2}C_{\text{net}}v_{C\text{net}}^2 + \frac{1}{2}Li_L^2 + \frac{1}{2}Cv_C^2 \quad (4a)$$

$$\dot{V} = k_v v_c i_{L\text{net}} - v_{c\text{net}}^2/Z_{\text{load}} - g\left(v_C\right)v_C - \frac{k_i v_c v_{c\text{net}}}{Z_{\text{load}}} - v_c^2/R \quad (4b)$$

following the Lyapunov theory [6], and noting that the first, second, and the fourth terms in 4(b) for $k_v \gg k_i$ and $i_{L\text{net}} \approx v_{c\text{net}}/Z_{\text{load}}$ and in the vicinity of the origin, the third term (which is positive) is greater than the fifth term given $\sigma > R^{-1}$ [2], the origin is not a stable equilibrium since $\dot{V} > 0$. Further, for higher values of v_C, when $g(v_C)$ and v_C have the same polarities [2], $\dot{V} < 0$. This change in polarity of $\dot{V}$ is indicative of the presence of a limit cycle.

For $i_N \neq 0$, this (60-Hz) limit cycle is affected depending on the frequency and amplitude of i_N and the bandwidth of the VOC. This is investigated using a numerical solution of (3) (and using a Poincaré map [6] to get discrete points) since an analytical solution is not feasible. Fig. 6(a1) and 6(a2) manifest that, as the noise (SNI) frequency approaches resonance frequency (60 Hz) of Z_{osc}, it yields the progressively higher peak amplitude of v_o that is more pronounced at higher noise amplitude and less pronounced with smaller VOC bandwidth. In contrast, Fig. 6(b1) and 6(b2), indicates that if one uses smaller VOC bandwidth for higher noise immunity, it comes at the price of an appreciable increase in time to reach the steady state of v_o, thereby yielding a slower inverter.

V. Impact of SNI on Stability of Two Parallel CFSIs

Section IV demonstrates that SNI in a CFSI leads to a loss of periodicity of the 60-Hz limit cycle (i.e., the CFSI output cannot be synchronized to the desired 60-Hz output frequency

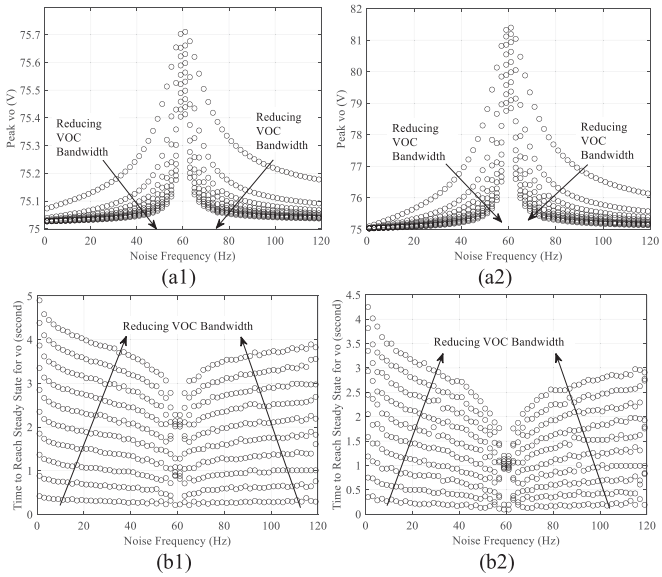

Fig. 6. (a1), (a2) and (b1), (b2) Effects of variation in noise (SNI) frequency on the peak amplitude of v_o and on the time to reach the steady state for v_o, respectively, for varying VOC bandwidth and different noise amplitudes [10% ((a1), (b1)) and 100% ((a2), (b2)) of the current feedback]. For bandwidth variation, the R, L, and C parameters of Z_{osc} are varied from the nominal values of 10 Ω, 500 μH, and 14.07 μF to 10 Ω, 50 μH, and 140.7 μF, while ensuring the same VOC resonant frequency of 60 Hz.

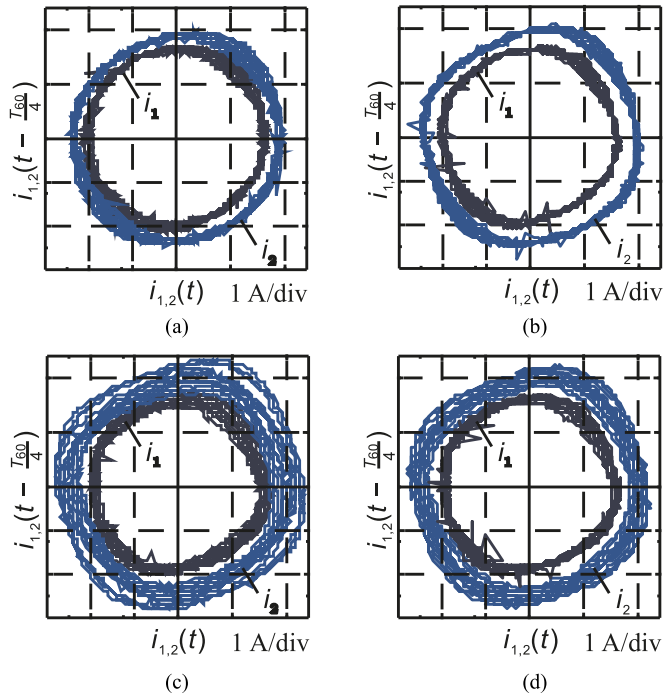

Fig. 7. Phase-plane plots of the two parallel (i.e., networked) CFSIs: (a), (b) without SNI for OL and VOC implementations, (c) SNI in i_1, and (d) SNIs of equal magnitudes (at frequencies of ±3 Hz of 60 Hz) in i_1 and i_2.

even though the VOC is tuned for 60 Hz). Subsequently, in this section, we first explore what happens to the synchronism of the two CFSIs (i.e., $N = 2$ in Fig. 2) connected in a parallel configuration if one of the CFSI is subjected to a SNI.

Fig. 7(a) and 7(b) demonstrates the experimental phase-plane plots of $i_1(t)$ and $i_2(t)$ against $i_1(t - T_{60}/4)$ and $i_2(t - T_{60}/4)$, respectively, when the CFSIs work without SNI under OL conditions and with VOC. In contrast, Fig. 7(c) demonstrates the impact of the SNI only in i_1 on the dynamics of the parallel CFSI. The SNI frequency is set at 57 Hz, which is close to the bandwidth of the VOC filter, and the noise amplitude is set at 100% of the i_1 obtained without noise.

It is evident from the phase-plane plots involving i_1 and i_2 that the periodicity of the 60-Hz limit cycle is affected by the SNI and more importantly, the dynamics of the two inverter currents are different. Since v_o is common output voltage for both the CFSIs comprising the same Z_{net}, the additional difference in the two currents is attributed to the differences in v_1 and v_2. This, following (1), implies that not only is each CFSI not synchronized to a common 60-Hz output frequency, but the two CFSIs are also not synchronized to each other in the sense of (1). Thus, VOC operation is compromised.

Fig. 7(d) shows experimentally the impact of SNI in i_1 and i_2 corresponding to CFSIs 1 and 2. The magnitude of the injected noise is kept the same as that used to obtain Fig. 6(c). However, the frequencies of SNIs for i_1 and i_2 are set at 60 ± 3 Hz. The results demonstrate, following arguments made for Fig. 6(c), that, SNIs lead to loss of periodicity of the noise-free 60-Hz limit cycle and loss of synchronism between the two CFSIs per (1). This result also indicates, following [1], that, even if the equal-magnitude SNIs for i_1 and i_2 were injected at the same frequency (that is higher than the Nyquist sampling frequencies of the two digital VOC controllers) but sampled by the controllers at different frequencies, then, for specific sampling rates, the aliased signals can have 60 ± 3 Hz components, which will have the same effect, as shown in Fig. 6(d).

Next, in Fig. 8, we demonstrate experimentally the time-domain responses corresponding to the four separate cases considered in Fig. 7. Fig. 8(a) and 8(b) shows the noise-free OL and VOC results for the two CFSIs. Fig. 8(c) and 8(d) shows the performances when SNI is injected in i_1 and SNIs of equal magnitude are injected in i_1 and i_2, respectively. The latter results clearly demonstrate the loss of 60-Hz periodicity of the CFSI dynamics and the difference between i_1 and i_2, validating the loss of synchronism between the two CFSIs.

VI. Kalman Filter-Based Estimation to Mitigate the Impact of SNI in a CFSI

Given that the feedback signal (i_1) is tampered, a static Kalman filter-based estimation algorithm is used to suppress the effect of SNI. This is achieved, following [1], by replacing the tampered measurement of i_1 with its estimation. The estimation is obtained by minimizing the estimated error's expected value subject to predetermined observation noise covariances [1]. This, so that, in the steady state, one obtains $\mathbb{E}(\xi_{k|k-1}) = 0$, with $\{\xi \in \mathbb{R} : \xi_{k|k-1} = \hat{x}_{k|k-1} - x_k\}$, i.e., $\{\hat{x}_{k|k-1}, \hat{x}_{k+1|k}, \ldots, \hat{x}_{k+n|k+n-1}\} \rightarrow \{x_k, x_{k+1}, \ldots, x_{k+n}\}$, where x_k stands for measured states of the CFSI for the kth sampling cycle while $\hat{x}_{k|k-1}$ represents the *a posteriori* estimate of x for the kth sampling cycle.

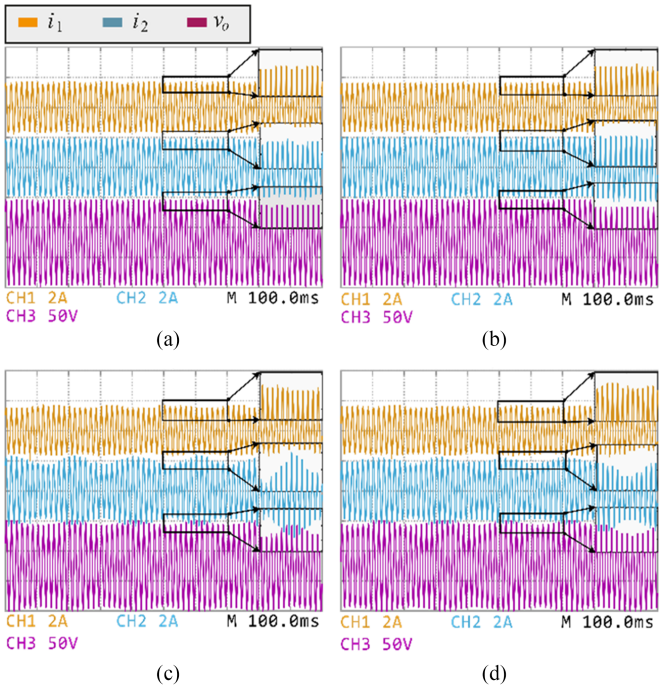

Fig. 8. Time-domain performances of the two parallel CFSIs (with zoom): (a), (b) without SNI for OL and VOC implementations, (c) SNI in i_1, and (d) SNIs of equal magnitudes (at frequencies of ± 3 Hz of 60 Hz) in i_1 and i_2.

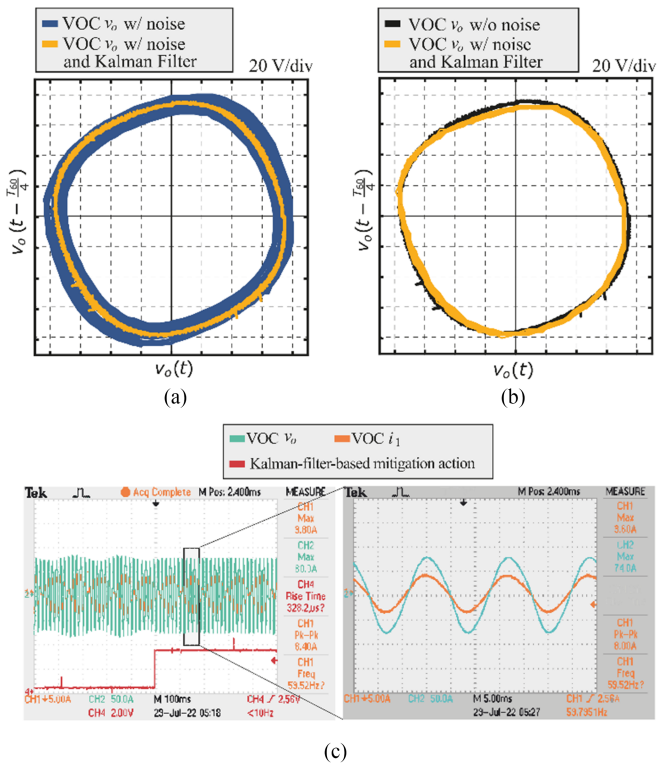

Fig. 9. (a) Performance of the VOC-based CFSI with and without Kalman filtering-based estimation of i_1, which is tampered using a SNI at 57 Hz. (b) Closeness of the performance of the VOC-based CFSI using estimation to the nominal case when there is no SNI in i_1. (c) Time-domain performance demonstrates how the activation of estimation stabilizes the CFSI dynamics.

Fig. 9(a) experimentally demonstrates the efficacy of the VOC using the Kalman filter-based estimation. It is evident that the VOC is able to stabilize the 60-Hz limit cycle using the estimated i_1. Fig. 9(b) demonstrates the closeness of the performance of the CFSI using estimation-based VOC (when i_1 feedback is tampered) to the nominal case when no noise is injected.

VII. Conclusion

This letter illustrates experimentally along with parametric analysis that, while VOC-based CFSIs nominally self-synchronize to a common output frequency (e.g., 60 Hz) without coordinated communication, which is a desired feature, their global synchronization is vulnerable to malicious SNI in their local feedback(s). The results indicate that, depending on the SNI frequency and amplitude, given a set of VOC parameters, the ability of a VOC-based CFSI to ensure a stable 60-Hz limit cycle is compromised. For a parallel CFSI configuration, comprised of two inverters, it is found that SNI affects not only the stability of a common 60-Hz limit cycle, but the synchronization of the parallel CFSIs as well. It is found that even if SNI is injected into the feedback of only one CFSI, it eventually affects the dynamics of the noise-free CFSI as well given the coupling of the CFSIs via the power network. An additional result suggests that even if SNIs of equal magnitude are injected at the same frequency (which is greater than the Nyquist sampling frequencies of the two digital VOC controllers) and sampled by the controllers at different sampling rates; if the aliased signals are in the close vicinity to the common 60-Hz frequency, then the synchronism and stability of the limit cycle can still be affected negatively. Finally, a potential noise mitigation approach using the Kalman filter-based estimation method for a CFSI is described. Further, experimental results detailing the method's efficacy are provided, illustrating that the mitigation method aids the VOC methodology in maintaining CFSI synchronization. It can be conjectured that, the issues explored in this letter for VOC-based CFSI are relevant to other classes of self-synchronizing inverters (e.g., those based on other forms of Kuramoto oscillators) and variations [7], [8], [9] of core VOC outlined in [2] and interesting subjects of future investigation.

Appendix A
Supporting Equations for Section II [2]

The network of N oscillators coupled through

$$i(s) = (i_1(s) \dots i_N(s))^T = Y(s)(v_1(s) \dots v_N(s))^T = Y(s)\, v(s) \quad \text{(A1)}$$

with the admittance matrix

$$Y(s) = \alpha(s) I_N + \beta(s) \Gamma \quad \text{(A2)}$$

where $\alpha(s),\ \beta(s) \in \mathbb{C}$, I_N is an $N \times N$ identity matrix, and Γ is the network Laplacian [2], synchronizes in the sense of (1)

$$\lim_{t \to \infty} v_j(t) - v_k(t) = 0 \ \ \forall j,\ k = 1, \cdots N \quad (1)$$

provided that

$$\|\mathcal{F}(\zeta(s), \beta(s)\lambda_2)\|_2 \sigma < 1. \quad \text{(A3)}$$

In (A3), λ_2 is the smallest positive eigenvalue of Γ

$$\zeta(s) := Z_{\text{osc}}(s)/1 + \alpha(s) Z_{\text{osc}}(s) \tag{A4}$$

and

$$\mathcal{F}(\zeta(s), \beta(s)\lambda_2) = \tilde{\gamma}(I_N + Z_{\text{osc}}(s) Y(s))^{-1} Z_{\text{oscm}}(s) \tag{A5}$$

where $\tilde{\gamma}$ is the differential L_2 gain of $g(v)$ in Fig. 1 and $Z_{oscm}(s) = Z_{osc}(s) \cdot I_N$.

APPENDIX B
LIENARD'S THEOREM [2], [4] FOR SECTION II

Consider the system

$$\ddot{v} + r(v)\dot{v} + m(v) = 0 \quad (2)$$

where $v : [0, \infty) \to \Re$ and $r(v),\ m(v) : \Re \to \Re$ are differentiable with respect to v. The functions $r(v)$ and $m(v)$ are even and odd, respectively. In addition, define

$$R(v) := \int_0^v r(\tau)\, d\tau. \tag{B1}$$

The system in (2) has a unique and stable limit cycle provided

$$m(v) > 0\ \forall v \tag{B2}$$

$$R(v) \text{ has one positive zero for some } v = p \tag{B3}$$

$$R(v) < 0 \text{ when } 0 < v < p \tag{B4}$$

$$R(v) \text{ monotonically increases for } v > p,\ \lim_{v\to\infty} R(v) = \infty. \tag{B5}$$

REFERENCES

[1] N. Gajanur, M. D. R. Greidanus, S. K. Mazumder, and M. A. Abbaszada, "Impact and mitigation of high-frequency side-channel noise intrusion on the low-frequency performance of an inverter," *IEEE Trans. Power Electron.*, vol. 37, no. 10, pp. 11481–11485, Oct. 2022, doi: 10.1109/TPEL.2022.3170885.

[2] B. B. Johnson, "Control, analysis, and design of distributed inverter systems," Ph.D. dissertation, Dept. Elect. Comput. Eng., Univ. Illinois, Urbana-Champaign, IL, USA, 2013.

[3] A. Barua and M. A. Al Faruque, "Special session: Noninvasive sensor-spoofing attacks on embedded and cyber-physical systems," in *Proc. IEEE 38th Int. Conf. Comput. Des.*, 2020, pp. 45–48, doi: 10.1109/ICCD50377.2020.00024.

[4] S. H. Strogatz, *Nonlinear Dynamics and Chaos: With Applications to Physics, Biology, Chemistry, and Engineering*, 1st Ed., Studies in nonlinearity. Boulder, CO, USA: Westview Press, Jan. 2001.

[5] A. Nabae, I. Takahashi, and H. Akagi, "A new neutral-point-clamped PWM inverter," *IEEE Trans. Ind. Appl.*, vol. IA-17, no. 5, pp. 518–523, Sep. 1981, doi: 10.1109/TIA.1981.4503992.

[6] A. H. Nayfeh and B. Balachandran, *Applied Nonlinear Dynamics*, New York, NY, USA: Wiley, 1995.

[7] G. -S. Seo, M. Colombino, I. Subotic, B. Johnson, D. Groß, and F. Dörfler, "Dispatchable virtual oscillator control for decentralized inverter-dominated power systems: Analysis and experiments," in *Proc. IEEE Appl. Power Electron. Conf. Expo.*, 2019, pp. 561–566, doi: 10.1109/APEC.2019.8722028.

[8] M. Lu, S. Dutta, V. Purba, S. Dhople, and B. Johnson, "A grid-compatible virtual oscillator controller: Analysis and design," in *Proc. IEEE Energy Convers. Congr. Expo.*, 2019, pp. 2643–2649, doi: 10.1109/ECCE.2019.8913128.

[9] M. A. Awal, H. Yu, H. Tu, S. M. Lukic, and I. Husain, "Hierarchical control for virtual oscillator based grid-connected and islanded microgrids," *IEEE Trans. Power Electron.*, vol. 35, no. 1, pp. 988–1001, Jan. 2020, doi: 10.1109/TPEL.2019.2912152.